Triphenylide-Based Molecular Solid – a New Candidate for a Quantum Spin-Liquid Compound

Supporting information

Aleš Štefančič[1,2], Gyöngyi Klupp[1], Tilen Knaflič[3], Dmitry S. Yufit[1], Gašper Tavčar[3], Anton Potočnik[3], Andrew Beeby[1], Denis Arčon[3,4,*]

[1]*Department of Chemistry, Durham University, Durham DH1 3LE, UK*

[2]*Jožef Stefan International Postgraduate School, Jamova 39, SI-1000 Ljubljana, Slovenia*

[3]*Jožef Stefan Institute, Jamova 39, SI-1000 Ljubljana, Slovenia*

[4]*Faculty of Mathematics and Physics, University of Ljubljana, Jadranska 19, SI-1000 Ljubljana, Slovenia*

Table of contents

Experimental

General

Since potassium triphenylide is a highly air and moisture sensitive salt all the synthesis and handling of the products were carried out under anaerobic conditions using Schlenk techniques and an argon-filled glove box (M-Braun MB200B, < 0.1 ppm H_2O and O_2). Triphenylene (Acros Organics, 98 %) was sublimed at 190 °C under static vacuum, and afterwards transferred and stored in a glove box. Potassium metal (Alfa Aesar, 99.95%, sealed under argon) was kept in a glove box and used as received. 1,2-dimethoxyethane (DME) (Acros Organics, 99+%) and *n*-pentane (Acros Organics, for analysis) were dried under sodium/benzophenone, kept in gas-tight glass vessel and distilled prior to use. All reactions were carried out in custom-build H-reaction vessel, which allowed solvent manipulation and crystal growth in separate parts of the vessel.

Synthesis of $K_2(C_{18}H_{12})_2$(DME) *(1)*

9 ml of DME was condensed on top of 158.7 mg (0.695 mmol) of triphenylene and 26.9 mg (0.688 mmol) of potassium metal placed in one of the two sides of H-vessel. The solution, which immediately turned into lavender-purple color, was stirred at RT until all potassium metal was consumed/dissolved (2 days). Subsequently the solution was decanted into second side of the vessel and the crystal growth was achieved by layering the solution with *n*-pentane. After 4 days black needle-like crystals with purple luster were observed. Crystals were washed three times with new *n*-pentane in course of three days. Sample was evacuated under dynamic vacuum (9.0×10^{-4} mbar) for 2 h in order to remove solvents. Elongated rectangle shape crystals were obtained, which turned into deep purple powder upon grinding. Reaction yield was 164.3 mg (76%). Elemental analysis calculated for $K_2(C_{18}H_{12})_2(C_4H_{10}O_2)$ gives: C 76.88, H 5.48; mean of found C 76.16, H 5.49 in units of (m/m %). The stoichiometry obtained from elemental analysis is $K_{2.00\text{-}2.24}(C_{18}H_{12})_2DME_{1.04\text{-}1.07}$. Phase purity of the bulk was confirmed by powder X-ray diffraction (Fig. S1).

Elemental analysis

CHN analysis was performed with an Exeter Analytical CE-440 Elemental Analyzer. The sample was sealed into a pre-weighed tin capsule to prevent oxidation (an empty tin capsule was also sealed inside the glove box for argon mass difference correction).

Structural analysis

Single crystal XRD analysis: Single crystals were selected under the microscope inside the glove box, placed into 2 cm long and 0.7 mm diameter silica capillaries, and afterwards air-tightly sealed by wax. The X-ray single crystal data for $K_2(C_{18}H_{12})_2$(DME) were collected at 120 and 293 K with a Bruker SMART 6000 diffractometer (fine-focus tube, graphite monochromator, Monocap optics, λMoKα radiation, λ = 0.71073 Å) equipped with a Cryostream (Oxford Cryosystems) open-flow nitrogen cryostat. The structure was solved by direct method and refined by full-matrix least squares on F^2 for all data using Olex2[1] and SHELXTL[2] software. All non-hydrogen atoms were refined anisotropically. All hydrogen atoms were placed in the calculated positions and refined in riding mode with U_{iso} = 1.2 U_{eq}(C).

Crystal data for $K_2(C_{18}H_{12})_2$(DME) ***(1)*** at T = 120 K: $C_{40}H_{34}K_2O_2$, M_r = 624.87, orthorhombic, a = 10.2589(3), b = 15.7908(5), c = 18.7420(6) Å, V = 3036.13(16) Å^3, space group $P2_12_12_1$, Z = 4, λ = 0.71073

Å, $\rho_{calc.}$ = 1.367 g cm^{-3}, μ = 0.349 mm^{-1}, 35146 reflections measured, 7338 independent reflections (R_{int} = 0.0563). Final R_1 = 0.0591 (3145 reflections with I>4σ (I)) and wR_2 = 0.0888 (all data). The goodness of fit on F^2 was 1.008.

Crystal data for $K_2(C_{18}H_{12})_2$(DME) ***(1)*** at T = 293 K: $C_{40}H_{34}K_2O_2$, M_r = 624.87, orthorhombic, a = 10.3376(4), b = 15.9197(6), c = 18.8668(8) Å, V = 3104.9(2) Å^3, space group $P2_12_12_1$, Z = 4, λ = 0.71073 Å, $\rho_{calc.}$ = 1.337 g cm^{-3}, μ = 0.341mm^{-1}, 34570 reflections measured, 7478 independent reflections (R_{int} = 0.1345). Final R_1 = 0.1546 (3145 reflections with I>4σ (I)) and wR_2 = 0.1713 (all data). The goodness of fit on F^2 was 1.021.

Powder XRD analysis: Powder sample of ***(1)*** was filled into 0.5 mm diameter Special Glass (Capillary Tube Supplies Ltd) capillary and sealed under Ar atmosphere. Powder X-ray diffraction data were collected at ambient temperature with a Bruker D8 Advance diffractometer (Mo $K\alpha$ λ = 0.7093 Å, 2Θ = 1 to 30°) operating in transmission mode equipped with LYNXEYE XE energy-dispersive one-dimensional detector.

A structural model obtained from singe crystal X-ray diffraction at 293 K was refined to powder diffraction profile using EXPO2014 suite[3]. Lattice constants and agreement factors of Rietveld refinements: 293 K; a = 10.3421(3), b = 15.9290(6), c = 18.8825(6) Å, V = 3110.70(17) Å^3, R_{wp} = 5.512%, R_{exp} = 2.487%. Since the R_{wp} of refinements with K1 and K2 occupations fixed to 1 and with free K occupations do not differ significantly, we conclude that the composition of **(1)** is $K_2(C_{18}H_{12})_2$(DME).

Optical spectroscopy

Ultraviolet-visible-near infrared spectroscopy: A DME solution of ***(1)*** was prepared and measured in a 1 mm light pass air tight quartz cuvette in transmission in the range 200-1100 nm by an ATI Unicam UV-visible spectrometer. The peaks below 400 nm correspond to the excitations of the triphenylene core. A nujol mull from solid ***(1)*** was prepared in an Ar filled glove box with oxygen and water levels below 0.1 ppm. The nujol suspension was placed between two glass slides and measured in a custom-made air tight sample holder in transmission (T). The optical density was calculated according to $O.\ D.$ = -lg$T$. A slight difference in the spectra of the solid and the solution can arise because of a different distortion of the molecules and because the vibronic bands are more smeared out in the solid.

Infrared spectroscopy: KBr pellets were prepared from ***(1)*** inside an Ar filled glove box with oxygen and water levels below 1 ppm. The pellets were measured in transmission with 2 cm^{-1} resolution by a Bruker Alpha spectrometer located also inside the glove box. Measurements with 0.5 cm^{-1} resolution did not reveal any further splitting. The preparation of pellets induced the oxidation of a small amount of sample, which could be avoided by using an ATR (attenuated total reflection) setup for measuring in the abovementioned spectrometer. The obtained spectrum, free of pristine triphenylene is shown in Fig. S4.

Raman spectroscopy: Solid samples were measured on the same capillaries as used for powder X-ray diffraction experiments. For excitation a 785 nm diode laser and a 532 nm frequency doubled Nd:YAG laser has been used with a power of 70 μW and 80 μW, respectively, at the focus on the sample. Higher laser power was found to cause irreversible discoloration of the sample. The spectra have been measured with a Horiba Jobin Yvon LabRAM HR confocal spectrometer in back scattering. The spectra obtained with the 785 nm (532 nm) laser were acquired using a 600 gr/mm (1800 gr/mm) grating resulting in 0.6 cm^{-1}

(~0.4 cm^{-1}) sampling interval. The spectrum of the DME solution of ***(1)*** in a quartz cuvette was obtained with 785 nm excitation using the same setup.

DFT calculation

Single point calculations were performed both on the SVWN/3-21G level and on the B3LYP/6-31G* level with HyperChem Release 7.03. The former method is using the Slater exchange functional[4,5,6] and the correlation functional of Vosko, Wilk, and Nusair[7] and the local spin density approximation with the basis localized on atoms, while the latter is a hybrid exchange correlation functional method[8] with a better basis set localized on the atoms. The geometry of the monoanions was fixed to that obtained from single crystal diffraction for Tri1 and Tri2 to obtain information about the molecular ions in the crystal. The two methods gave the same shape of the MOs and the splitting pattern of orbitals, however, energy difference of the MOs calculated with SVWN/3-21G method agree better with the experimental excitation energies. A test calculation on naphthalide anions also showed that SVWN/3-21G method provides better agreement with the peak positions of literature UV-visible spectroscopy measurements[9].

SQUID magnetometry

Temperature-dependent magnetic susceptibility (χ) measurements at ambient-pressure were performed on a 29.9 mg sample in a sealed thin-wall quartz ampule at an applied field of 1 T between 1.8 and 300 K with a Quantum Design SQUID MPMS magnetometer. The temperature dependence of the magnetization, *M*, of the sample was measured at applied field of 100 Oe under both zero-field-cooling (ZFC) and field-cooling (FC) protocols and is shown on Figure S6. Correction for the diamagnetic core contributions of K^+(-14.9×10^{-6} emu mol^{-1}), triphenylene, (-153.08×10^{-6} emu mol^{-1}) and DME (-63.46×10^{-6} emu mol^{-1}) were applied to all datasets.

EPR spectroscopy

The EPR measurements on single crystal were performed on a Bruker Elexsys e580 X-band spectrometer using a Varian TEM104 dual-cavity resonator. An Oxford Instruments ESR900 cryostat and an Oxford Instruments ITC503 temperature controller made temperature dependence measurements possible with temperature stability better than ± 0.05 K. Spectra were measured on cooling between room temperature and 4 K. The complementary EPR intensity calibration was done only for a powder sample using a homemade L-band resonator, by comparing the EPR signal of the sample to that of the calibrated DPPH (2,2-diphenyl-1-picrylhydrazyl) standard. The susceptibility of the DPPH sample was separately determined by SQUID magnetometry. We note that in X-band EPR experiments on single crystals we were unable to calibrate the signal intensity due to the unreliable determination of a very small single crystal mass (typically, much less than 1 mg) – these highly air-sensitive samples have to be strictly handled in an inert atmosphere of argon filled glove box.

Supplementary Tables

Table S1. Comparison of the bond distances in $K_2(C_{18}H_{12})_2$(DME) collected at 120 K and 293 K, along with C-C bond distances in pristine triphenylene collected at 150 K[10]. The last column contains the hapticity defined by the coordination bond lengths, where the sum of carbon Van der Waals radius (1.7 Å) and potassium ionic radius (1.78 Å) was taken as a cut-off value, and the position of potassium cation, defined by cation to plane centroid to plane angle.

Bond	Bond distances (Å) of ***(1)*** at 120 K	Bond distances(Å) of ***(1)*** at 293 K	Bond distances (Å) of triphenylene at 150 K	Hapticity and angle
C1-C2	1.376(3)	1.381(8)	1.382(5)	
C2-C3	1.398(4)	1.396(9)	1.394(6)	
C3-C4	1.406(4)	1.391(8)	1.380(5)	
C4-C15	1.393(3)	1.390(8)	1.414(5)	
C15-C16	1.480(3)	1.478(7)	1.475(5)	
C16-C5	1.409(3)	1.407(8)	1.412(5)	
C5-C6	1.381(3)	1.370(9)	1.375(5)	
C6-C7	1.390(3)	1.389(8)	1.393(5)	
C7-C8	1.370(3)	1.368(7)	1.380(5)	
C8-C17	1.409(3)	1.403(7)	1.415(5)	
C17-C18	1.465(3)	1.456(7)	1.469(4)	
C18-C9	1.398(3)	1.392(8)	1.408(5)	
C9-C10	1.393(3)	1.395(9)	1.383(5)	
C10-C11	1.402(3)	1.386(9)	1.391(5)	
C11-C12	1.376(3)	1.375(8)	1.379(5)	
C12-C13	1.442(3)	1.436(8)	1.415(5)	
C13-C14	1.420(3)	1.412(8)	1.470(5)	
C14-C1	1.443(3)	1.443(8)	1.409(5)	
C14-C15	1.438(3)	1.412 (7)	1.411(5)	
C13-C18	1.447(3)	1.461(7)	1.415(4)	
C16-C17	1.414(3)	1.421(5)	1.412(4)	
K1-C1	3.369(2)	3.404(6)		
K1-C2	3.151(3)	3.177(6)		η^5
K1-C3	3.045(3)	3.076(6)		79.9°

K1-C4	3.182(2)	3.223(5)		
K1-C15	3.420(2)	3.458(5)		
K1-C9	3.452(2)	3.472(6)		
K1-C10	3.323(2)	3.346(6)		
K1-C11	3.141(2)	3.164(6)		η^6
K1-C12	3.124(2)	3.157(6)		81.6°
K1-C13	3.311(2)	3.346(5)		
K1-C18	3.460(2)	3.469(5)		
K2-C1	3.232(2)	3.289(6)		η^3
K2-C2	3.157(3)	3.205(6)		80.6°
K2-C3	3.303(3)	3.319(6)		
K2-C9	3.218(2)	3.243(6)		
K2-C10	3.155(2)	3.172(6)		
K2-C11	3.148(2)	3.178(6)		η^6
K2-C12	3.206(2)	3.243(6)		86.6°
K2-C13	3.289(2)	3.327(5)		
K2-C18	3.295(2)	3.341(5)		
C1a-C2a	1.366(3)	1.375(9)	1.382(5)	
C2a-C3a	1.386(4)	1.368(9)	1.394(6)	
C3a-C4a	1.394(4)	1.391(9)	1.380(5)	
C4a-C15a	1.402(3)	1.395(8)	1.414(5)	
C15a-C16a	1.460(3)	1.471(7)	1.475(5)	
C16a-C5a	1.417(3)	1.420(8)	1.412(5)	
Ca5-C6a	1.381(4)	1.367(10)	1.375(5)	
C6a-C7a	1.388(4)	1.369(10)	1.393(5)	
C7a-C8a	1.375(4)	1.387(9)	1.380(5)	
C8a-C17a	1.412(3)	1.416(7)	1.415(5)	
C17a-C18a	1.469(3)	1.453(7)	1.469(4)	
C18a-C9a	1.395(3)	1.394(8)	1.408(5)	
C9a-C10a	1.405(3)	1.393(9)	1.383(5)	
C10a-C11a	1.391(4)	1.383(11)	1.391(5)	
C11a-C12a	1.377(4)	1.388(10)	1.379(5)	

C12a-C13a	1.440(3)	1.449(8)	1.415(5)	
C13a-C14a	1.429(3)	1.414(7)	1.470(5)	
C14a-C1a	1.441(3)	1.424(8)	1.409(5)	
C14a-C15a	1.429(3)	1.422(7)	1.411(5)	
C13a-C18a	1.436(3)	1.443(7)	1.415(4)	
C16a-C17a	1.414(3)	1.430(7)	1.412(4)	
K2-C9a	3.158(2)	3.208(6)		
K2-C10a	3.036(2)	3.066(6)		η^5
K2-C11a	3.204(2)	3.222(6)		77.9°
K2-C12a	3.458(2)	3.455(6)		
K2-C18a	3.446(2)	3.486(5)		
O1-K1	2.7156(15)	2.742(4)		
O2-K1	2.7951(16)	2.817(4)		
O2-K2	2.9007(17)	2.946(4)		
K1-K2	4.7159(8)	4.7410(18)		

Table S2. Bond length changes between triphenylide ions and the neutral triphenylene molecule[10] and out-of-plane displacements of C atoms of triphenylide ions. Values for Tri1 are given on the left, Tri2 on the right. The estimated standard deviations are given in parenthesis, providing the statistical verification of deformation of the radical anions.

bond	difference / Å	bond	difference / Å
C1-C2	-0.006(6)	C1a-C2a	-0.016(6)
C2-C3	0.004(7)	C2a-C3a	-0.008(7)
C3-C4	0.026(6)	C3a-C4a	0.014(6)
C4-C15	-0.021(6)	C4a-C15a	-0.012(6)
C15-C16	0.005(6)	C15a-C16a	-0.015(6)
C16-C5	-0.003(6)	C16a-C5a	0.005(6)
C5-C6	0.006(6)	Ca5-C6a	0.006(6)
C6-C7	-0.003(6)	C6a-C7a	-0.005(6)
C7-C8	-0.010(6)	C7a-C8a	-0.005(6)
C8-C17	-0.006(6)	C8a-C17a	-0.003(6)
C17-C18	-0.004(5)	C17a-C18a	0.000(5)
C18-C9	-0.010(6)	C18a-C9a	-0.013(6)
C9-C10	0.010(6)	C9a-C10a	0.022(6)
C10-C11	0.011(6)	C10a-C11a	0.000(6)
C11-C12	-0.003(6)	C11a-C12a	-0.002(6)
C12-C13	0.027(6)	C12a-C13a	0.025(6)
C13-C14	-0.050(6)	C13a-C14a	-0.041(6)
C14-C1	0.034(6)	C14a-C1a	0.032(6)
C14-C15	0.027(6)	C14a-C15a	0.018(6)
C13-C18	0.032(5)	C13a-C18a	0.021(5)
C16-C17	0.002(5)	C16a-C17a	0.002(5)

atom	z / Å	atom	z / Å
C1	0.076(2)	C1a	0.030(2)

C2	0.008(2)	C2a	-0.016(2)
C3	-0.081(2)	C3a	-0.065(2)
C4	-0.079(2)	C4a	-0.039(2)
C5	0.032(2)	C5a	0.096(2)
C6	0.0370(19)	C6a	0.082(2)
C7	0.0269(19)	C7a	-0.030(2)
C8	-0.0002(19)	C8a	-0.100(2)
C9	-0.072(2)	C9a	-0.015(2)
C10	-0.0644(19)	C10a	0.011(2)
C11	0.0120(19)	C11a	0.020(2)
C12	0.063(2)	C12a	0.026(2)
C13	0.040(2)	C13a	0.025(2)
C14	0.044(2)	C14a	0.023(2)
C15	-0.011(2)	C15a	0.010(2)
C16	0.000(2)	C16a	0.014(2)
C17	-0.008(2)	C17a	-0.053(2)
C18	-0.022(2)	C18a	-0.020(2)

Table S3. Vibrational frequencies (in cm^{-1}) of ***(1)*** detected by IR and Raman spectroscopy using 532 nm and 785 nm excitations compared to those of pristine triphenylene. The first column contains the irreducible representations previously assigned to the triphenylene peaks[11,12] and the assignment of the DME peaks. Please note that the assignment of the specific triphenylide peaks of ***(1)*** is only tentative. The last three columns tabulate the shift of the vibrational peaks (cm^{-1}) caused by the reduction of triphenylene.

irrep	$C_{18}H_{12}$ IR	$C_{18}H_{12}$ Raman	*(1)* IR	*(1)* Raman (532 nm)	*(1)* Raman (785 nm)	Shift IR	Shift Raman (532 nm)	Shift Raman (785 nm)
E'	407	409		401			-8	
A_1'		419		394	393		-25	-26
A_2''	420		412	414	414	-8		
E'	619	621	618	618		-1	-3	
A_1'	698	700		686	687		-14	-13
E''		710	664					
A_2''	740		697	697		-43		
E'	772	772	722			-50		
			732			-40		
E'	779	778	750			-29		
			762	759	763	-17	-19	-15
E''	849		843			-6		
E''	953							
A_2''	950							
E'	994			989				
E'	1005	1006	1000	998		-5	-8	
A_2'	1023		1018			-5		
E'	1051	1052	1027		1026	-24		-26
			1052	1052	1049	1	0	-3
A_1'	1061	1062		1037	1037		-25	-25
E'	1109	1110	1062			-47		
E'	1141	1143	1088		1086	-53		-57
			1106			-35		
E'	1145		1115			-30		

E'	1162	1159		1146			-13	
E'	1170	1171		1156			-15	
A_1'	1182	1181		1167			-14	
A_1'		1229		1228			-1	
E'	1243	1246	1219	1221		-24	-25	
			1232	1235		-11	-11	
A_2'	1255		1250			-5		
E'	1292		1268			-24		
E'	1299	1299	1277	1275		-22	-24	
A_1'	1340	1340		1333			-7	
$E' + A_2'$	1396		1343			-53		
$E' + A_1'$	1409		1368			-41		
E'	1433	1434		1352	1354		-82	-80
			1428	1430	1428	-5	-4	-6
A_1'	1458	1458	1458	1459			1	
E'	1497		1445	1439		-52		
			1467			-30		
A_1'		1547		1486	1482		-61	-65
E'	1578	1579		1536			-43	
E'	1603	1605	1560	1559		-43	-46	
E'		1616		1591			-25	
				1602			-14	
DME			2824					
DME			2889					
DME			2925					

Table S4: The fitting parameters of the spin-only susceptibility measured by EPR and by SQUID for the alternating spin chain and strong rung spin ladder models. The value for the spin-gap obtained from the low-temperature logarithmic linear fit of susceptibility data modelled by $\chi \propto T^{\frac{1}{2}} \exp(-\Delta/T)$ is also shown.

Alternating chain model			
Parameter	X-band EPR	L-band EPR	SQUID
Curie Constant (emu/mol K)	/	0.6 ± 0.1	0.48 ± 0.01
J (K)	268 ± 4	290 ± 13	298 ± 4
α	0.59 ± 0.02	0.50 ± 0.07	0.52 ± 0.02
Δ (K)	150 ± 20	190 ± 20	190 ± 20
Impurity percentage (%)	0.6 ± 0.2	0.7 ± 0.2	1.6 ± 0.1
T_c (K)	-1 ± 1	-1 ± 1	-1 ± 0.1
Strong rung ladder model			
Curie Constant (emu/mol K)	/	0.6 ± 0.1	0.50 ± 0.01
J_{rail} (K)	152 ± 6	130 ± 25	138 ± 8
J_{rung} (K)	226 ± 2	263 ± 6	269 ± 2
Δ (K)	130 ± 20	170 ± 20	170 ± 20
Impurity percentage (%)	0.6 ± 0.2	0.7 ± 0.2	1.6 ± 0.1
T_c (K)	-1 ± 1	-1 ± 1	-1 ± 0.1
$\chi \propto T^{\frac{1}{2}} \exp(-\Delta/T)$			
Δ (K)	120 ± 1	155 ± 2	141 ± 1

Supplementary Figures

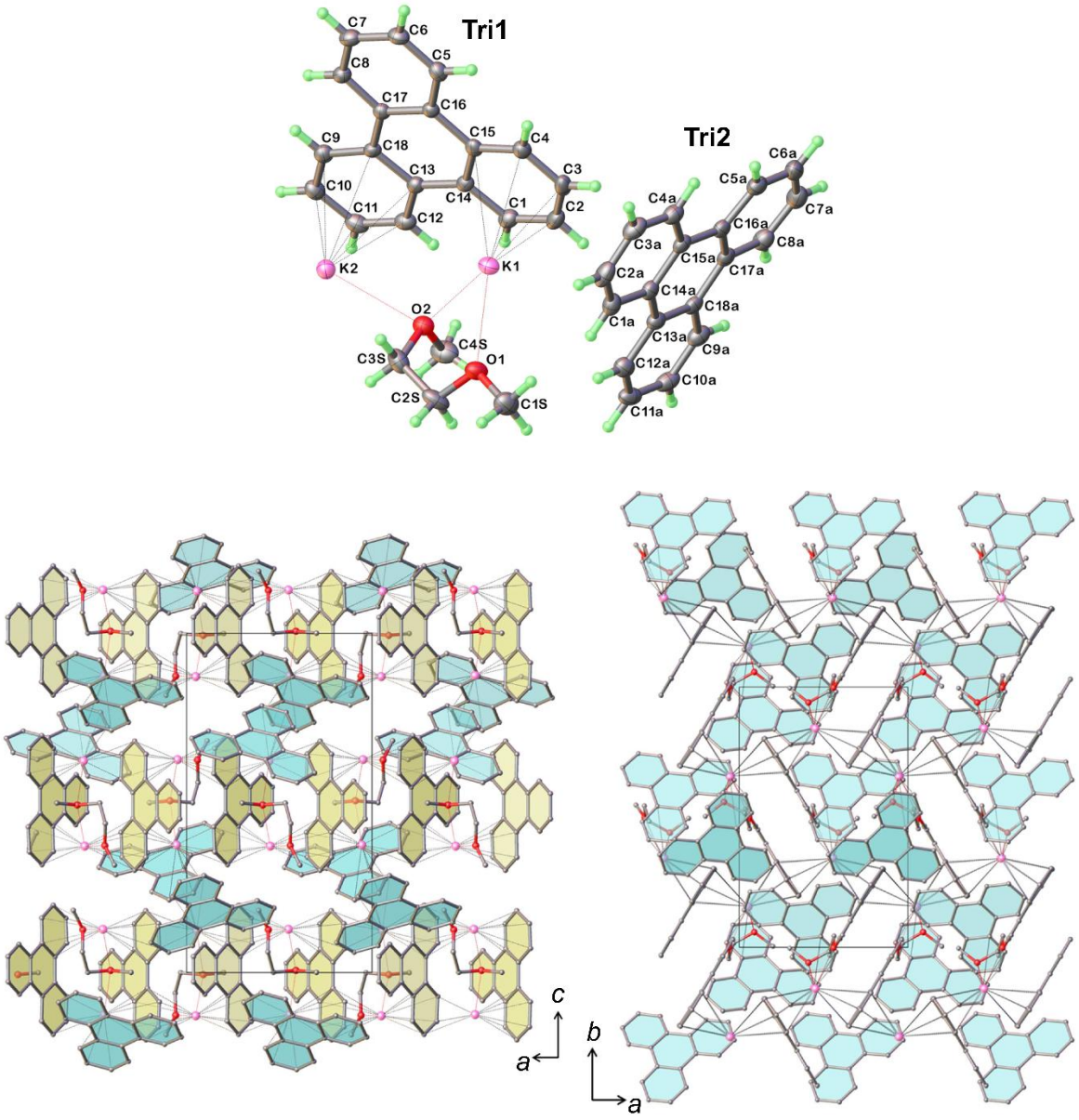

Figure S1. **(top)** Presentation of asymmetric part in the unit cell of $K_2(C_{18}H_{12})_2$(DME). Tri1 and Tri2 are presenting crystallographically independent triphenylene molecular ions. Black dotted and red dotted lines correspond to K – C and K –O coordination interactions respectively. Color code: grey, C; pale green H; lilac, K; red, O. **(bottom)** Projection of the crystal structure along the [010] (left) and along [001] (right) crystallographic direction. Color code: light yellow, Tri1; light cyan, Tri2.

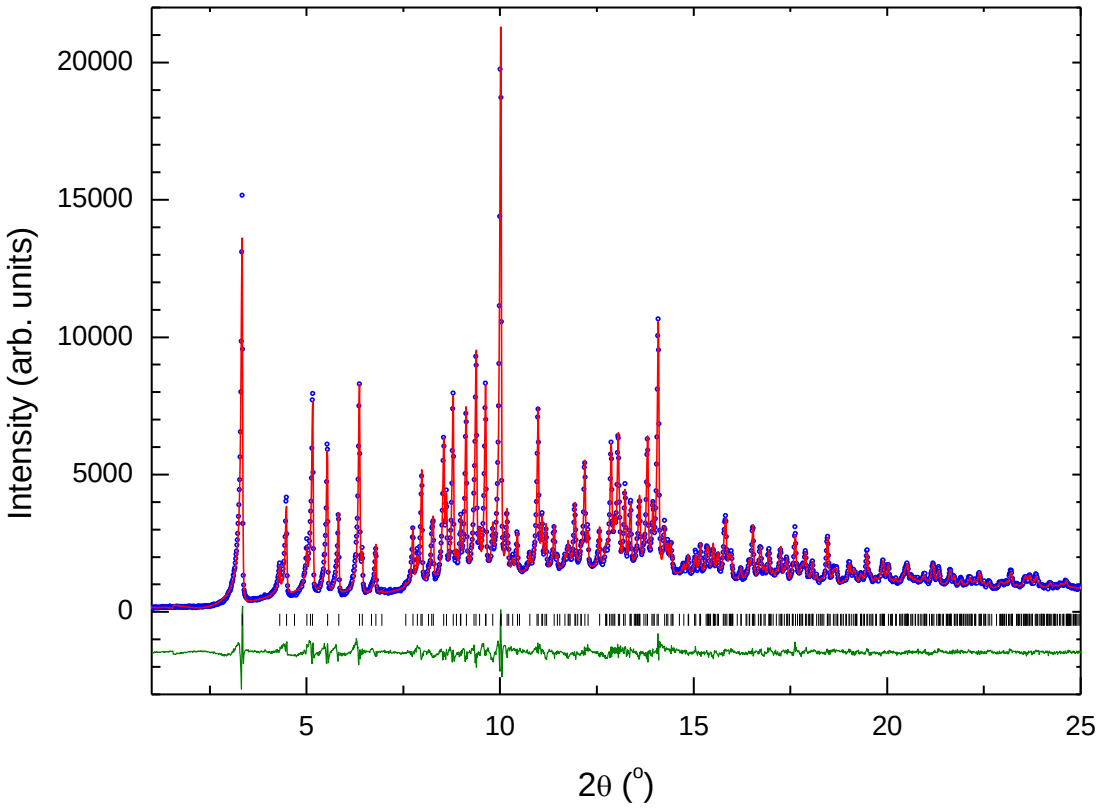

Figure S2: Powder X-ray diffraction profile of $K_2(C_{18}H_{12})_2$(DME). The experimentally obtained diffraction profile at ambient temperature (blue open circles), refinement based on the model obtained from single crystal X-ray diffraction at 293 K (red solid line), difference (olive green solid line) and predicted peak positions (black tick marks).

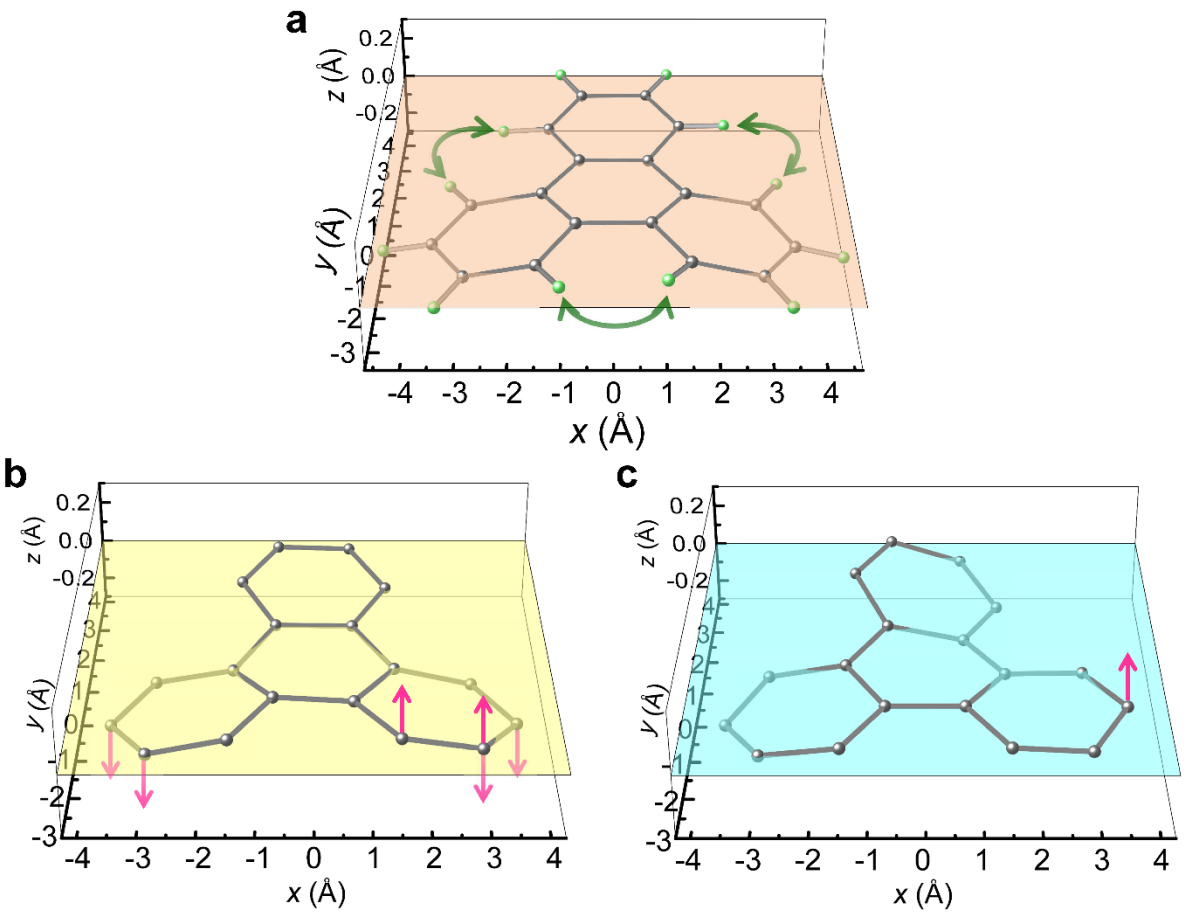

Figure S3: Out-of-plane distortion of neutral and charged triphenylene molecules. The coordinates of the atoms (C: grey, H: green) are shown compared to the mean plane of the molecule on an expanded axis. (**a**) The neutral triphenylene molecule in the pristine triphenylene crystal[10] with the crowding of bay hydrogens illustrated with olive arrows. (**b**) Tri1 and (**c**) Tri2 ions of $K_2(C_{18}H_{12})_2$(DME) with H atoms omitted for clarity. The bridgehead C atoms of the closest K – C distances are indicated with magenta arrows showing the attractive K – π interaction contributing to the distortion of the molecules.

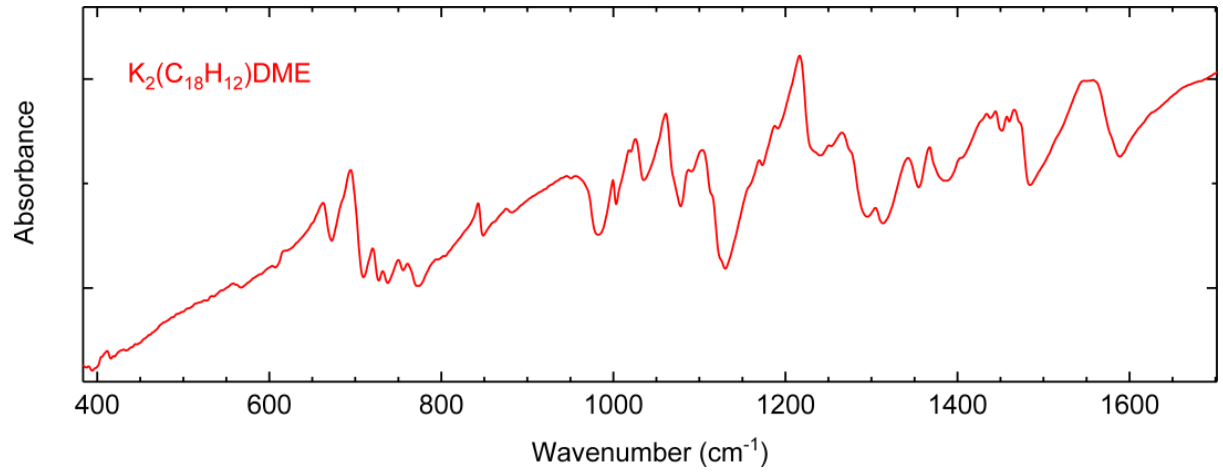

Figure S4: The ATR infrared spectrum of $K_2(C_{18}H_{12})_2$DME at room temperature.

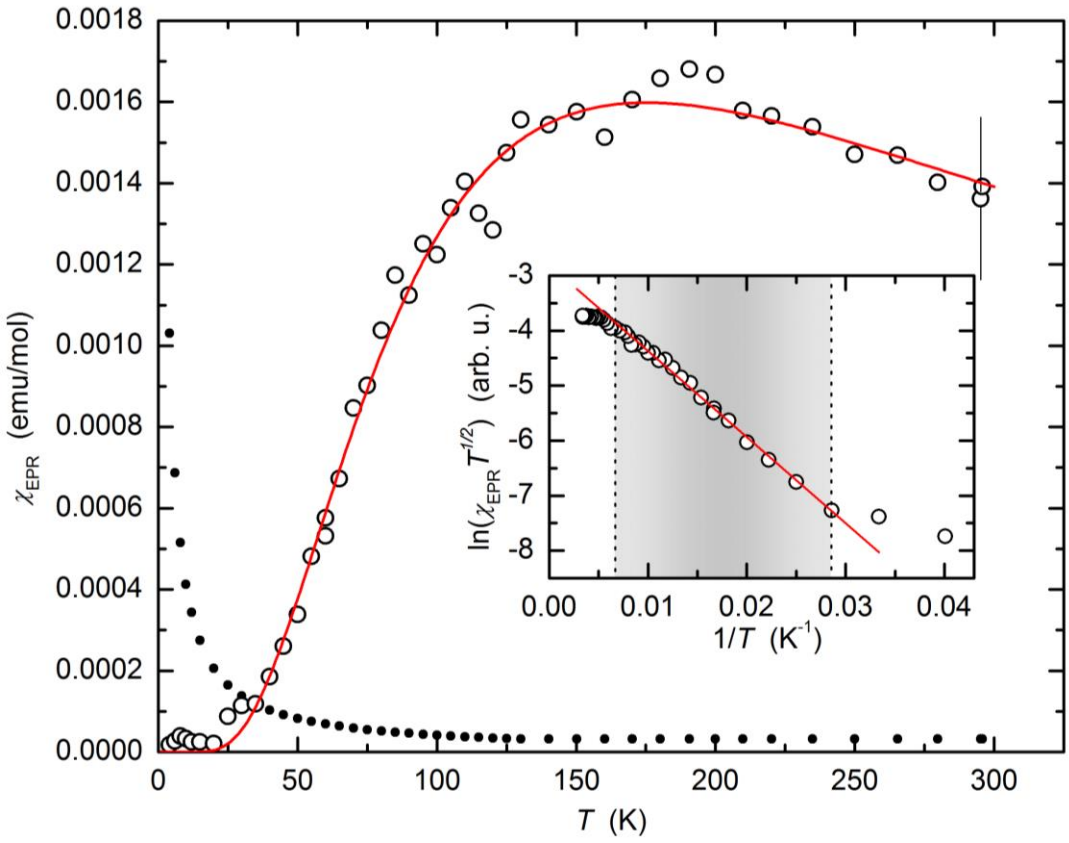

Figure S5: Temperature dependence of spin susceptibility as measured by L-band EPR (open circles) with $T_{max}^{EPR} \cong 175$ K. The solid black circles present EPR intensity of the impurity line, obtained by deconvoluting the EPR signal with two Lorentzian line-shapes. The solid red line shows a fit to strong rung ladder model. The inset shows linear fit to the natural logarithm of spin-only EPR susceptibility versus the inverse temperature. Data highlighted within the grey area are used to extract the spin gap $\Delta = 155 \pm 2$ K. The error bar at room temperature applies to all data points.

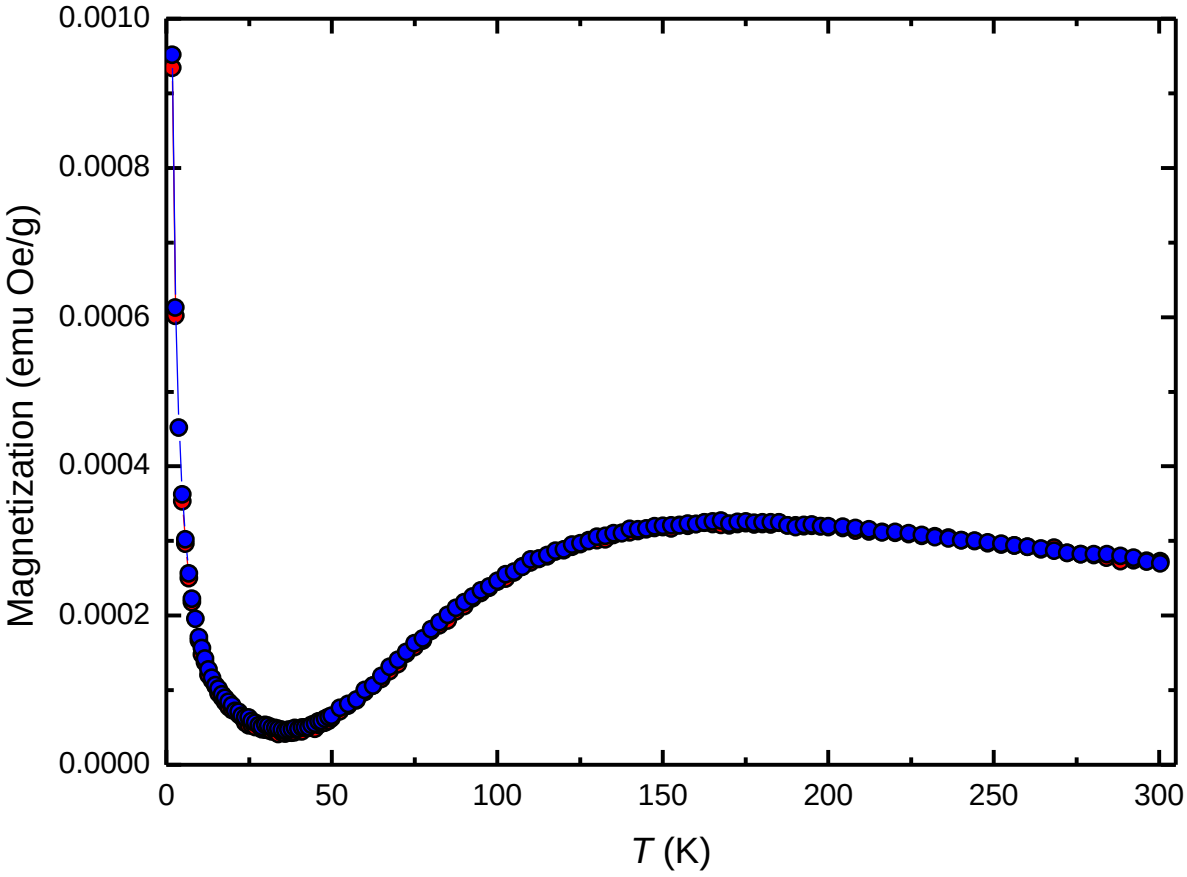

Figure S6: Temperature dependence of static spin magnetization of $K_2(C_{18}H_{12})_2(DME)$ measured by SQUID in ZFC (red circles) and FC (blue circles) protocol upon heating at a magnetic field of 10 mT.

References

(1) Dolomanov, O. V.; Bourhis, L. J.; Gildea, R. J.; Howard, J. A. K.; Puschmann, H., Olex2: A complete structure solution, refinement and analysis program. *J. Appl. Cryst.* **2009**, *42*, 339.

(2) Sheldrick, G. M., A short history of SHELX. *Acta Crystallogr. A* **2008**, *64* (1), 112.

(3) Altomare, A.; Camalli, M.; Cuocci, C.; Giacovazzo, C.; Moliterni, A.; Rizzi, R., EXPO2013: a kit of tools for phasing crystal structures from powder data. *J. Appl. Crystallogr.* **2013**, *46* (4), 1231.

(4) Hohenberg, P.; Kohn, W., Inhomogeneous Electron Gas. *Phys. Rev.* **1964**, *136*, B864.

(5) Kohn, W.; Sham, L. J., Self-Consistent Equations Including Exchange and Correlation Effects. *Phys. Rev.* **1965,** *140*, A1133.

(6) Slater, J. C. *The Self-Consistent Field for Molecular and Solids, Quantum Theory of Molecular and Solids*. McGraw-Hill: New York, 1974. Vol. 4.

(7) Vosko, S. H.; Wilk, L.; Nusair, M., Accurate spin-dependent electron liquid correlation energies for local spin density calculations: a critical analysis. *Can. J. Phys.* **1980**, *58*, 1200.

(8) Becke, A. D., Density-functional thermochemistry. III. The role of exact exchange. *J. Chem. Phys.* **1993**, *98*, 5648.

(9) Shida, T.; Iwata, S., Electronic spectra of ion radicals and their molecular orbital interpretation. III. Aromatic hydrocarbons. *J. Am. Chem. Soc.* **1973**, *95*, 3473.

(10) Collings, J. C.; Roscoe, K. P.; Thomas, R. L.; Batsanov, A. S.; Stimson, L. M.; Howard, J. A. K.; Marder, T. B., Arene-perfluoroarene interactions in crystal engineering. Part 3. Single-crystal structures of 1 : 1 complexes of octafluoronaphthalene with fused-ring polyaromatic hydrocarbons. *New J. Chem.* **2001**, *25* (11), 1410.

(11) Schettino, Infrared and Raman spectra of crystalline triphenylene and triphenylene-d12 and normal coordinates calculations. V. *J. Mol. Spectrosc.* **1970**, *34*, 78.

(12) Keszthelyi, T.; Balakrishnan, G.; Wilbrandt, R.; Yee, W. A.; Negri, F., Evidence of Dynamical Jahn−Teller Effect on Triphenylene Radical Cation: Resonance Raman Spectrum and ab Initio Quantum-Chemical Calculations. *J. Phys. Chem. A* **2000**, *104*, 9121.